Inorg. Chem. **2009**, *48*, 2614−2625

Effect of Imidazole and Phenolate Axial Ligands on the Electronic Structure and Reactivity of Oxoiron(IV) Porphyrin π-Cation Radical Complexes: Drastic Increase in Oxo-Transfer and Hydrogen Abstraction Reactivities

Akihiro Takahashi, Takuya Kurahashi, and Hiroshi Fujii*

Institute for Molecular Science and Okazaki Institute for Integrative Bioscience, National Institutes of Natural Sciences, and Department of Functional Molecular Science, The Graduate University for Advanced Studies, Myodaiji, Okazaki 444-8787, Japan

Received November 5, 2008

To study the effect of axial ligands on the electronic structure and reactivity of compound I of peroxidases and catalases, oxoiron(IV) porphyrin π-cation radical complexes with imidazole, 2-methylimidazole, 4(5)-methylimidazole, and 3-fluoro-4-nitrophenolate as the axial ligands were prepared by ozone oxidation of iron(III) complexes of 5,10,15,20-tetramesitylporphyrin (TMP) and 2,7,12,17-tetramethyl-3,8,13,18-tetramesitylporphyrin (TMTMP). These complexes were fully characterized by absorption, ^{1}H, ^{2}H, and ^{19}F NMR, electron paramagnetic resonance (EPR), and electrospray ionization mass spectrometry (ESI-MS) spectroscopy. The characteristic absorption peak of compound I at approximately 650 nm was found to be a good marker for estimation of the electron donor effect from the axial ligand. The axial ligand effect did not change the porphyrin π-cation radical state, the a_{2u} state of the TMP complexes, or the a_{1u} radical state of both the TMTMP complexes and compound I. The ferryl iron and porphyrin π-cation radical spins were effectively transferred into the axial ligands for the a_{2u} complexes but not for the a_{1u} complexes. Most importantly, the reactivity of the oxoiron(IV) porphyrin π-cation radical complex was drastically increased by the imidazole and phenolate axial ligands. The reaction rate for cyclooctene epoxidation was increased 100- to 400-fold with axial coordination of imidazoles and phenolate. A similar increase was also observed for the oxidation of 1,4-cyclohexadiene,*N*,*N*-dimethyl-*p*-nitroaniline and hydrogen peroxide. These results suggest extreme enhancement of the reactivity of compound I by the axial ligand in heme enzymes. The functional role of axial ligands on the compound I in heme enzymes is discussed.

Introduction

Oxoiron(IV) porphyrin π-cation radical species in peroxidases and catalases, called compound I, is known as a reactive intermediate of these enzymes.[1,2] It is also believed that compound I is formed as a reactive intermediate in the catalytic cycles of cytochrome P450.[3] Although these enzymes share a common reactive intermediate, the reactivity of compound I differs from enzyme to enzyme. The compound I in cytochrome P450 directly transfers a single oxygen atom to a variety of substrates, while those in peroxidases and catalases carry out oxidation of organic substrates, such as amines and phenols, and oxidation of hydrogen peroxide to water and oxygen gas, respectively.[1−3] It is generally accepted that the diverse functions of

* To whom correspondence should be addressed. E-mail: hiro@ims.ac.jp.

(1) (a) Hersleth, H.-P.; Ryde, U.; Rydberg, P.; Görbitz, C. H.; Andersson, K. K. *J. Inorg. Biochem.* **2006**, *100*, 460–476. (b) Watanabe, Y.; Fujii, H. In *Metal-Oxo and Metal-Peroxo Species in Catalytic Oxidations*; Meunier, B., Ed.; Springer: New York, 2000; Vol. 97, pp 61−89. (c) Dunford, H. B. *Heme Peroxidases*; Wiley-VCH: New York, 1999.

(2) (a) Kirkman, H. N.; Gaetani, G. F. *Trends Biochem. Sci.* **2007**, *32*, 44–50. (b) Putnam, C. D.; Arvai, A. S.; Bourne, Y.; Tainer, J. A. *J. Mol. Biol.* **2000**, *296*, 295–309. (c) Schonbaum, G. R.; Chance, B. In *The Enzymes*; Boyer, P. D., Ed.; Academic Press: New York, 1976; Vol. 13, pp 363−408.

(3) (a) Denisov, I. G.; Makris, T. M.; Sliger, S. G.; Schlichting, I. *Chem. Rev.* **2005**, *105*, 2253–2278. (b) Oritz de Montellano, P. R. *Cytochrome P450. Structure, Mechanism, and Biochemistry*, 2nd ed.; Plenum Publishing Corporation: New York, 1995. (c) Watanabe, Y.; Groves, J. T. In *The Enzymes*; Sigman, D. S., Ed.; Academic Press: New York, 1992; Vol. 20, pp 405−452.

10.1021/ic802123m CCC: $40.75
Published on Web 02/13/2009

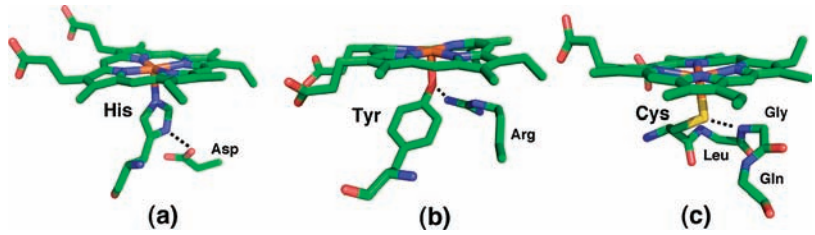

Figure 1. Active site structures of (a) peroxidase (HRP, PDB file 1DZ9), (b) catalase (*BL*-CAT, PDB file 2A9E), and (c) cytochrome P450 (Cytochrome $P450_{cam}$, PDB file 1HCH).

compound I are controlled by heme environmental structures, such as porphyrin peripheral structures, heme axial ligands, and protein structures around heme.

One significant structural difference in these heme enzymes is the heme axial ligand.[1−3] As shown in Figure 1, histidine and tyrosine residues (imidazole and phenolate) are coordinated to the heme iron as axial ligands in peroxidases, other than chloroperoxidase (CPO), and catalases, respectively. In cytochrome P450 and CPO, a cysteine residue (thiolate) is the heme axial ligand. The amino acids that serve as the axial ligands are highly conserved in these heme enzymes, suggesting some functional roles in these enzyme functions. In the reaction cycles of these enzymes, the axial ligand can affect both the formation of compound I and the reaction of compound I with the substrate. The effect of the axial ligand on the rate of compound I formation has been studied by mutation of the aspartic acids that interact with the proximal histidine residues in peroxidases; the mutations weakened the electron donor effect of the proximal histidines, drastically decreasing the rates of compound I formation.[1,4] A similar axial ligand effect was also observed for synthetic heme enzyme model complexes. The rate of heterolytic cleavage of the O−O bond of iron bound *m*-chloroperbenzoate, which leads to formation of the compound I model complex, increased as the electron donor effect of the axial imidazole ligand increased.[5] These mutation and synthetic enzyme model studies demonstrate that an increase in the electron donor effect of the axial ligand enhances the rate of compound I formation.

The axial ligand also modulates the electronic structure and reactivity of compound I. The electron paramagnetic resonance (EPR) studies of compound I in peroxidases and catalases indicated that the axial ligand changes the intramolecular spin coupling contant between the ferryl iron and the porphyrin radical spins.[6−11] Catalytic oxidation studies using synthetic iron(III) porphyrin complexes with imidazoles, phenolates, and thiolates as axial ligands suggested that the axial ligands have a significant effect on the reactivity and selectivity of compound I.[12−17] For example, in the catalytic competitive oxidation of cyclooctane/cyclooctene, the imidazole axial ligand produced greater product yields than the thiolate axial ligand. On the other hand, the thiolate axial ligand favored hydroxylation, whereas the imidazole axial ligand preferentially yielded epoxidation.[17] Recently, a pronounced axial ligand effect on the rate of styrene epoxidation was found by synthetic compound I model complexes with various axial anion ligands, such as chloride, fluoride, acetate, and so on.[18] More recently, the axial ligand effect was also studied in detail with other synthetic compound I model systems, as well as with density-functional theory (DFT) calculations.[19,20] Although these results clearly show the axial ligand effect on the electronic structure and reactivity of compound I, it is unclear how the enzyme axial ligands (imidazole, phenolate, and thiolate) change the electronic state and the reactivity of compound I. This problem is due to different protein structures making it difficult to compare the reactivity of compound I in heme enzymes and to the absence of stable compound I model complexes with imidazole, phenolate, and thiolate axial ligands because of the rapid reduction of compound I model complexes by these axial ligands.

In previous studies, we reported the first preparation of oxoiron(IV) porphyrin π-cation radical complexes with

(4) (a) Smulevich, G.; Mauro, J. M.; Fishel, L. A.; English, A. M.; Kraut, J.; Spiro, T. G. *Biochemistry* **1988**, *27*, 5477–5485. (b) Goodin, D. B.; McRee, D. E. *Biochemistry* **1993**, *32*, 3313–3324.
(5) Yamaguchi, K.; Watanabe, Y.; Morishima, I. *J. Am. Chem. Soc.* **1993**, *115*, 4058–4065.
(6) Schluz, C. E.; Rutter, R.; Sage, J. T.; Debrunner, P. G.; Hager, L. P. *Biochemistry* **1984**, *23*, 4743–4754.
(7) (a) Rutter, R.; Hager, L. P. *J. Biol. Chem.* **1982**, *257*, 7958–7961. (b) Rutter, R.; Hager, L. P.; Dhonau, H.; Hendrich, M.; Valentine, M.; Debrunner, P. *Biochemistry* **1984**, *23*, 6809–6816.
(8) Benecky, M. J.; Frew, J. E.; Scowen, N.; Jones, P.; Hoffman, B. M. *Biochemistry* **1993**, *32*, 11929–11933.
(9) Patterson, W.; Polous, T. L.; Goodin, D. B. *Biochemistry* **1995**, *34*, 4342–4345.
(10) Ivancich, A.; Jouve, H. M.; Sartor, B.; Gaillard, J. *Biochemistry* **1997**, *36*, 9356–9364.
(11) Khindaria, A.; Aust, S. *Biochemistry* **1996**, *35*, 13107–13111.
(12) Traylor, T. G.; Lee, W. A.; Stynes, D. V. *J. Am. Chem. Soc.* **1984**, *106*, 755–764.
(13) (a) Dicken, C. M.; Woon, T. C.; Bruice, T. C. *J. Am. Chem. Soc.* **1986**, *108*, 1636–1643. (b) Beck, M. J.; Gopinath, E.; Bruice, T. C. *J. Am. Chem. Soc.* **1993**, *115*, 21–29.
(14) Battioni, P.; Renaud, J. P.; Bartoli, J. F.; Reina-Artiles, M.; Fort, M.; Mansuy, D. *J. Am. Chem. Soc.* **1988**, *110*, 8462–8470.
(15) Robert, A.; Loock, B.; Momenteau, M.; Meunier, B. *Inorg. Chem.* **1991**, *30*, 706–711.
(16) (a) Higuchi, T.; Uzu, S.; Hirobe, M. *J. Am. Chem. Soc.* **1990**, *112*, 7051–7052. (b) Suzuki, N.; Higuchi, T.; Urano, Y.; Kikuchi, K.; Uekusa, H.; Ohashi, Y.; Uchida, T.; Kitagawa, T.; Nagano, T. *J. Am. Chem. Soc.* **1999**, *121*, 11571–11572. (c) Urano, Y.; Higuchi, T.; Hirobe, M.; Nagano, T. *J. Am. Chem. Soc.* **1997**, *119*, 12008–12009.
(17) Ohno, T.; Suzuki, N.; Dokoh, T.; Urano, Y.; Kikuchi, K.; Hirobe, M.; Higuchi, T.; Nagano, T. *J. Inorg. Biochem.* **2000**, *82*, 123–125.
(18) (a) Gross, Z.; Nimri, S. *Inorg. Chem.* **1994**, *33*, 1731–1732. (b) Gross, Z.; Nimri, S.; Barzilay, C. M.; Simkhovich, L. *J. Biol. Inorg. Chem.* **1997**, *2*, 492–506.
(19) Song, W. J.; Ryu, Y. O.; Song, R.; Nam, W. *J. Biol. Inorg. Chem.* **2005**, *10*, 294–304.
(20) (a) Kuramochi, H.; Noodleman, L.; Case, D. A. *J. Am. Chem. Soc.* **1997**, *119*, 11442–11451. (b) de Visser, S. P.; Ogliaro, F.; Sharma, P. K.; Shaik, S. *Angew. Chem., Int. Ed.* **2002**, *41*, 1947–1951. (c) Kamachi, T.; Kouno, T.; Nam, W.; Yoshizawa, K. *J. Inorg. Biochem.* **2006**, *101*, 1464–1472. (d) Wang, R.; de Visser, S. P. *J. Inorg. Biochem.* **2007**, *101*, 1464–1472.

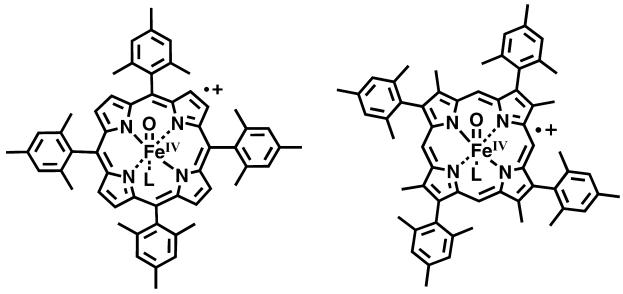

Figure 2. Structures of compound I model complexes prepared in this study.

imidazole and 4-nitrophenolate as models for compound-I of peroxidases and catalases.[21,22] Although the imidazole complex could be characterized with absorption, ^{1}H NMR, and resonance Raman spectroscopy, the 4-nitrophenolate complex was too unstable to characterize, except for its absorption spectrum. To fully characterize and compare reactivities, we comprehensively prepared oxoiron(IV) porphyrin π-cation radical complexes with imidazole (Im), 2-methylimidazole (2-MeIm), 4(5)-methylimidazole (5-MeIm), and 3-fluoro-4-nitrophenolate (3-F-4-NO_2-PhO) as axial ligands by ozone oxidation of iron(III) complexes of 5,10,15,20-tetramesitylporphyrin (TMP) and 2,7,12,17-tetramethyl-3,8,13,18-tetramesitylporphyrin (TMTMP), as shown in Figure 2. A stable catalase compound I model complex was synthesized with the 3-fluoro-4-nitrophenolate axial ligand. These imidazole and phenolate complexes were fully characterized using UV−visible absorption, ^{1}H, ^{2}H, and ^{19}F NMR, EPR, and electrospray ionization mass spectrometry (ESI-MS) spectroscopy. The TMTMP complexes more closely mimic the spectroscopic properties of compound I in peroxidases and catalases than the TMP complexes. The most important findings in this study were as follows: (1) that the porphyrin π-cation radical spin was significantly transferred in the axial imidazole (phenolate) and oxo ligands for the a_{2u} radical complex, but not for the a_{1u} radical complex, and (2) that the oxidation reactivity of oxoiron(IV) porphyrin π-cation radical complex was drastically increased, more than 400 times in the most significant case, with the coordination of imidazole and phenolate axial ligands, suggesting extremely reactive compound I in heme enzymes. On the basis of the present spectroscopic and kinetic studies, the functional roles of axial ligands on compound I in heme enzymes and catalytic oxidation reactions are discussed in the final section.

Results

Synthesis of Compound I Models. The oxoiron(IV) porphyrin π-cation radical complexes with imidazole and phenolate derivatives as axial ligands were prepared using

Scheme 1

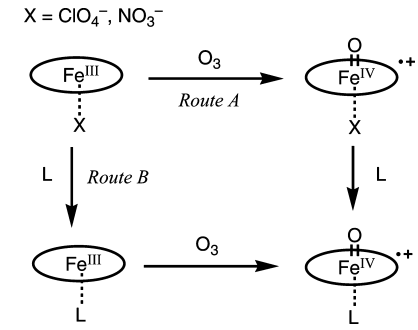

two alternative routes, as shown in Scheme 1. [(TMP$^{+\bullet}$)-Fe^{IV}O(L)](ClO$_4$) and [(TMTMP$^{+\bullet}$)Fe^{IV}O(L)](ClO$_4$), where L is Im, 2-MeIm, and 5-MeIm, were prepared from (TMP)-Fe^{III}(ClO$_4$) and (TMTMP)Fe^{III}(ClO$_4$) using route B, respectively. [(TMTMP$^{+\bullet}$)Fe^{IV}O(L)](ClO$_4$) also was prepared from (TMTMP)Fe^{III}(ClO$_4$) using route A. However, pure [(TMP$^{+\bullet}$)-Fe^{IV}O(L)](ClO$_4$) could not be prepared using route A because oxidation of (TMP)Fe^{III}(ClO$_4$) with ozone did not produce pure (TMP$^{+\bullet}$)Fe^{IV}O(ClO$_4$). To explore the effects of counter anions, we examined the preparation from nitrate iron(III) porphyrin complexes. In contrast to the perchlorate complexes, [(TMP$^{+\bullet}$)Fe^{IV}O(L)](NO$_3$) and [(TMTMP$^{+\bullet}$)Fe^{IV}O(L)]-(NO$_3$) were prepared from (TMP)Fe^{III}(NO$_3$) and (TMTMP)Fe^{III}(NO$_3$) using route A, respectively. On the other hand, route B was not effective, except for the case of TMTMPFe^{III}(NO$_3$) and 2-methylimidazole, because the addition of 1 equiv of the imidazole derivative to the nitrate complex did not afford its monoadduct complex but rather a mixture of the parent and bis-adduct complexes (Supporting Information, Figure S1). The oxoiron(IV) porphyrin π-cation radical complexes with imidazole derivatives, prepared from nitrate complexes using route A, were as stable as those prepared from perchlorate complexes at temperatures below 233 K in dichloromethane.

The preparation of oxoiron(IV) porphyrin π-cation radical complexes with phenolate derivatives (4-nitrophenolate, pentafluorophenolate, 3,4,5-trifluorophenolate, and 3-fluoro-4-nitrophenolate) as axial ligands was examined using route B for TMP and TMTMP complexes. The oxoiron(IV) porphyrin π-cation radical complexes with 4-nitrophenolate, 3,4,5-trifluorophenolate, and pentafluorophenolate were very unstable even at 183 K and quickly reduced to iron(III) porphyrin complexes with dissociation and decomposition of the axial phenol. However, the oxoiron(IV) porphyrin π-cation radical complex with 3-fluoro-4-nitrophenolate was stable enough for spectroscopic characterization at temperatures below 213 K in dichloromethane. In route A, the addition of 1 equiv of phenol derivatives to oxoiron(IV) porphyrin π-cation radical complex resulted in rapid reduction of the complex.

The preparation of oxoiron(IV) porphyrin π-cation radical complexes with thiolate axial ligands, as models for compound I of cytochrome P450 and CPO, using route A and B may be ineffective because of the sensitivity of iron(III) porphyrin thiolate complexes to moisture and dioxygen and

(21) Fujii, H.; Yoshimura, T.; Kamada, H. *Inorg. Chem.* **1997**, *36*, 6142–6143.
(22) Czarnecki, K.; Kincaid, J. R.; Fujii, H. *J. Am. Chem. Soc.* **1999**, *121*, 7953–7954.

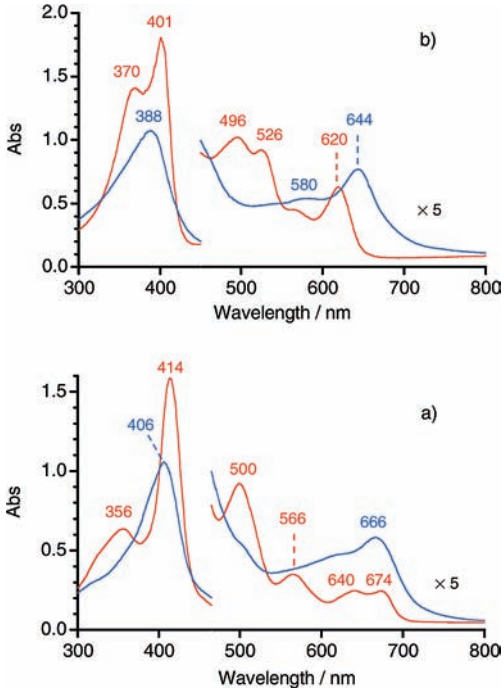

Figure 3. UV−visible absorption spectra of (P)Fe^{III}(3-F-4-NO_2-PhO), red lines, and ($P^{+\bullet}$)Fe^{IV}O(3-F-4-NO_2-PhO), blue lines, in dichloromethane (concentration 1.0×10^{-5} M, 1 cm path length cell) at −80 °C: (a) P = TMP, (b) P = TMTMP.

Table 1. UV-visible Absorption Spectral Data of [($P^{+\bullet}$)Fe^{IV}O(L)]X, in CH_2Cl_2 at −80°C

porphyrin	L	X	λ/nm	ref
TMP	ClO_4^-		403, 660	
	NO_3^-		401, 666	
	Im	ClO_4^-, NO_3^-	403, 667	
	2-MeIm	ClO_4^-, NO_3^-	403, 667	
	5-MeIm	ClO_4^-, NO_3^-	404, 667	
	3-F-4-NO_2-PhO		406, 666	
TMTMP	ClO_4^-		387, 621	
	NO_3^-		391, 630	
	$C_6H_5CO_2^-$		396, 645	
	Im	ClO_4^-, NO_3^-	394, 643	
	2-MeIm	ClO_4^-, NO_3^-	389, 646	
	5-MeIm	ClO_4^-, NO_3^-	394, 643	
	3-F-4-NO_2-PhO		388, 644	
	4-NO_2-PhO		392, 655	21

also because of the reducing ability of thiolate. Further modification will be required to prepare these complexes.

Characterization of Compound I Models. Figure 3 shows the UV−visible absorption spectra of ($TMP^{+\bullet}$)Fe^{IV}O(3-F-4-NO_2-PhO) and ($TMTMP^{+\bullet}$)Fe^{IV}O(3-F-4-NO_2-PhO) prepared from route B. The absorption maxima of the spectra are listed in Table 1. The absorption spectral features of ($TMTMP^{+\bullet}$)Fe^{IV}O(3-F-4-NO_2-PhO) were close to those of compound I of catalases (Table 2).[10,23,24] While ($TMP^{+\bullet}$)Fe^{IV}O(3-F-4-NO_2-PhO) slowly decomposed to (TMP)Fe^{III}(3-F-4-NO_2-PhO) in dichloromethane at −80 °C ($k_{decomp} = 3.3 \times 10^{-4}$ s^{-1}), ($TMTMP^{+\bullet}$)Fe^{IV}O(3-F-4-NO_2-PhO) was stable for a few hours under the same conditions.

Table 2. Absorption Spectra and EPR Data for Compound I of Peroxidases and Catalases

enzyme	axial ligand	λ/nm	EPR	ref
HRP	His	400, 651	∼ 2	6, 25
ASP	His	404, 650	3.27, 1.99	9, 26
LiP	His	408, 650	3.42, 2.00	11, 27
MnP	His	406, 650		28
CIP	His	402, 658		29
CPO	Cys	367, 688	2.00, 1.73, 1.64	7, 30
BL-CAT	Tyr	400, 656	1.96 (1.98)	10, 23
Eo-CAT	Tyr	402, 657		24
Pm-CAT	Tyr	655	∼2	10
Ml-CAT	Tyr		3.32, ∼2	8

The UV−visible absorption spectra of [($TMP^{+\bullet}$)Fe^{IV}O(L)](NO_3) and [($TMTMP^{+\bullet}$)Fe^{IV}O(L)](NO_3), where L is Im, 2-MeIm, and 5-MeIm, are shown in Supporting Information, Figures S2 and S3. As summarized in Table 1, the axial coordination of imidazole derivatives did not change the peak positions for the TMP complexes but did change them for the TMTMP complexes. The absorption spectral features of [($TMTMP^{+\bullet}$)Fe^{IV}O(L)](NO_3) resembled those of compound I of peroxidases more closely than those of [($TMP^{+\bullet}$)Fe^{IV}O(L)](NO_3) (Table 2).[25−30] Similar complexes with perchlorate anions were also prepared, and the peak positions were the same as those observed with nitrate anions.

Figure 4 shows the ^{1}H NMR spectra of ($TMP^{+\bullet}$)Fe^{IV}O(3-F-4-NO_2-PhO) and ($TMTMP^{+\bullet}$)Fe^{IV}O(3-F-4-NO_2-PhO) in dichloromethane-d_2 at −80 °C. The ^{1}H NMR signals were assigned using deuterium-labeled compounds, signal intensities, and comparisons with those of previously characterized oxoiron(IV) porphyrin π-cation radical complexes.[31] ($TMP^{+\bullet}$)Fe^{IV}O(3-F-4-NO_2-PhO) showed a pyrrole proton signal at −13.7 ppm, the *m*-proton of the meso mesityl group at 71.7 ppm, the *o*-methyl protons at 25.4 and 26.9 ppm, and the *p*-methyl protons at 11.3 ppm. The separation of the *o*-methyl signals reflected the coordination of two different axial ligands: oxo and phenolate. The large downfield shift of the meso mesityl protons indicated an unpaired electron in the a_{2u} porphyrin π-orbital, a_{2u} porphyrin π-cation radical state. On the other hand, ($TMTMP^{+\bullet}$)Fe^{IV}O(3-F-4-NO_2-PhO) showed a large downfield shift of the pyrrole methyl signal at 101.9 ppm and a small shift of the meso proton signal at −1.0 ppm. The small paramagnetic shift of the meso proton signal for ($TMTMP^{+\bullet}$)Fe^{IV}O(3-F-4-NO_2-PhO) clearly indicated an unpaired electron in the a_{1u} porphyrin π-orbital, a_{1u} porphyrin π-cation radical state. These ^{1}H NMR shifts are summarized in Tables 3 and 4.

Figure 5 shows the ^{1}H NMR spectra of [($TMP^{+\bullet}$)Fe^{IV}O(L)](ClO_4), where L is Im, 2-MeIm, and 5-MeIm, in dichloromethane-d_2 at −60 °C. The ^{1}H NMR shifts of [($TMP^{+\bullet}$)Fe^{IV}O(L)](ClO_4) are summarized in Table 3. The

(23) Browett, W. R.; Stillman, M. J. *Biochim. Biophys. Acta* **1980**, *623*, 21–31.
(24) Hara, I.; Ichise, N.; Kojima, K.; Kondo, H.; Ohgiya, S.; Matsuyama, H.; Yumoto, I. *Biochemistry* **2007**, *46*, 11–22.
(25) Dunford, H. B. *Adv. Inorg. Biochem.* **1982**, *4*, 41–68.
(26) Lad, L.; Mewies, M.; Raven, E. L. *Biochemistry* **2002**, *41*, 13774–13781.
(27) Renganathan, V.; Gold, M. H. *Biochemistry* **1986**, *25*, 1626–1631.
(28) Wariishi, H.; Akileswaran, L.; Gold, M. H. *Biochemistry* **1988**, *27*, 5365–5370.
(29) Anderson, M. B.; Hsuanyu, K.; Welinder, K. G.; Scheider, P.; Dunford, H. P. *Acta Chem. Scand.* **1991**, *45*, 1080–1086.
(30) Palcic, M. M.; Rutter, R.; Araiso, T.; Hager, L. P.; Dunford, H. B. *Biochem. Biophys. Res. Commun.* **1980**, *94*, 1123–1127.
(31) (a) Fujii, H. *J. Am. Chem. Soc.* **1993**, *115*, 4641–4648. (b) Fujii, H.; Ichikawa, K. *Inorg. Chem.* **1992**, *31*, 1110–1112.

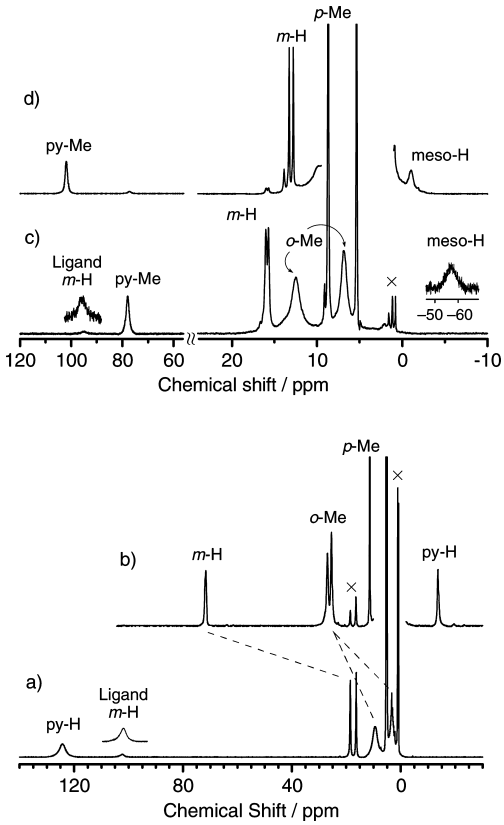

Figure 4. ^{1}H NMR spectra of iron porphyrin phenolate complexes in dichloromethane-d_2 at −80 °C: (a) (TMP)Fe^{III}(3-F-4-NO_2-PhO), (b) ($TMP^{+\bullet}$)Fe^{IV}O(3-F-4-NO_2-PhO), (c) (TMTMP)Fe^{III}(3-F-4-NO_2-PhO), (d) ($TMTMP^{+\bullet}$)Fe^{IV}O(3-F-4-NO_2-PhO).

large downfield shifts of the meso mesityl protons of [($TMP^{+\bullet}$)Fe^{IV}O(L)](ClO_4) indicated the a_{2u} porphyrin π-cation radical states, as the case of ($TMP^{+\bullet}$)Fe^{IV}O(3-F-4-NO_2-PhO). The ^{1}H NMR shifts of [($TMP^{+\bullet}$)Fe^{IV}O(2-MeIm)](ClO_4) were similar to those of [($TMP^{+\bullet}$)Fe^{IV}O(Im)](ClO_4) and [($TMP^{+\bullet}$)Fe^{IV}O(5-MeIm)](ClO_4), but the ^{1}H NMR signals of [($TMP^{+\bullet}$)Fe^{IV}O(2-MeIm)](ClO_4) were broader and were split at −90 °C (Figure 5c,d). This was because the rotation of the axially bound 2-methylimidazole along the Fe−N(2-MeIm) axis was hindered by a steric interaction between the 2-methyl group of 2-methylimidazole and the *o*-methyl group of the meso mesityl group. The ^{1}H NMR spectra of [($TMP^{+\bullet}$)Fe^{IV}O(L)](NO_3) were identical to those of [($TMP^{+\bullet}$)Fe^{IV}O(L)](ClO_4) (Supporting Information, Figure S4).

The ^{1}H NMR spectra of [($TMTMP^{+\bullet}$)Fe^{IV}O(L)](ClO_4), where L is Im, 2-MeIm and 5-MeIm, in dichloromethane-d_2 at −80 °C are shown in Supporting Information, Figure S5. The ^{1}H NMR spectra of [($TMTMP^{+\bullet}$)Fe^{IV}O(L)](ClO_4) indicated their a_{1u} porphyrin π-cation radical states. Unlike [($TMP^{+\bullet}$)Fe^{IV}O(2-MeIm)](ClO_4), the rotation of the 2-MeIm in [($TMTMP^{+\bullet}$)Fe^{IV}O(2-MeIm)](ClO_4) is not hindered. This is because the *o*-methyl group of the pyrrole β-mesityl group in TMTMP is farther from the iron center than that of the meso mesityl group in TMP. The ^{1}H NMR spectra of [($TMTMP^{+\bullet}$)Fe^{IV}O(L)](NO_3) are similar to those of [($TMTMP^{+\bullet}$)Fe^{IV}O(L)](ClO_4) (Supporting Information, Figure S6). The temperature dependence of ^{1}H NMR signals for [($TMP^{+\bullet}$)Fe^{IV}O(L)](ClO_4) and [($TMTMP^{+\bullet}$)Fe^{IV}O(L)](ClO_4) showed normal Curie's law behavior (Supporting Information, Figure S7).

Direct evidence for the coordination of imidazole derivatives to oxoiron(IV) porphyrin π-cation radical complexes was obtained by the ^{2}H NMR spectra of iron-bound deuterium-labeled imidazole derivatives (Figure 6). The ^{2}H NMR shifts are summarized in Table 5, together with the NMR shifts of iron-bound imidazole signals of oxoiron(IV) and iron(III) porphyrin complexes (Supporting Information, Figures S8 and S9). The paramagnetic shifts of the ^{2}H NMR signals of the deuterium-labeled imidazole derivatives clearly show their coordination to the ferryl iron site as axial ligands. The ^{2}H NMR signals for the 2- and 4-positions of the iron-bound imidazole derivative show upfield shifts, while those for the 5-position show downfield shifts. With substitutions of the 2-positions with methyl groups, the ^{2}H NMR signals of the methyl groups were observed downfield. The ^{2}H NMR paramagnetic shifts of iron-bound imidazole signals for [($TMP^{+\bullet}$)Fe^{IV}O(L)](ClO_4) were larger than those of [($TMTMP^{+\bullet}$)Fe^{IV}O(L)](ClO_4). Direct evidence for the phenolate binding to oxoiron(IV) porphyrin π-cation radical complexes was also obtained from their ^{19}F NMR spectroscopy (Supporting Information, Figure S10).

Figure 7 shows the EPR spectra of [($TMP^{+\bullet}$)Fe^{IV}O(2-MeIm)](ClO_4) and [($TMTMP^{+\bullet}$)Fe^{IV}O(2-MeIm)](ClO_4) at 4 K. [($TMP^{+\bullet}$)Fe^{IV}O(2-MeIm)](ClO_4) showed the EPR signals at $g = 4.47$, 3.45, and 1.97, which were similar to those of ($TMP^{+\bullet}$)Fe^{IV}O(ClO_4).[32] The EPR spectra of [($TMP^{+\bullet}$)Fe^{IV}O(2-MeIm)](ClO_4) were typical of those of $S = 3/2$ systems, indicating strong ferromagnetic interactions between ferryl iron ($S = 1$) and the porphyrin π-cation radical ($S = 1/2$). The EPR spectra of [($TMP^{+\bullet}$)Fe^{IV}O(Im)](ClO_4), [($TMP^{+\bullet}$)Fe^{IV}O(5-MeIm)](ClO_4), and ($TMP^{+\bullet}$)Fe^{IV}O(3-F-4-NO_2-PhO) were very close to that of [($TMP^{+\bullet}$)Fe^{IV}O(2-MeIm)](ClO_4), suggesting similar spin interactions (Table 3 and Supporting Information, Figures S11 and S12).

The EPR spectrum of [($TMTMP^{+\bullet}$)Fe^{IV}O(2-MeIm)](ClO_4) differed from that of [($TMP^{+\bullet}$)Fe^{IV}O(2-MeIm)](ClO_4) but was similar to that of [($TMTMP^{+\bullet}$)Fe^{IV}O(MeOH)](ClO_4) reported previously (Figure 7b).[32] The EPR spectra of [($TMTMP^{+\bullet}$)Fe^{IV}O(Im)](ClO_4) and [($TMTMP^{+\bullet}$)Fe^{IV}O(5-MeIm)](ClO_4) were similar to that of [($TMTMP^{+\bullet}$)Fe^{IV}O(2-MeIm)](ClO_4), but the $g_\perp$ values were changed by the axial imidazole ligand (Table 4 and Supporting Information, Figure S11). These EPR spectra were interpreted as a weak ferromagnetic interaction between ferryl iron ($S = 1$) and the porphyrin π-cation radical ($S = 1/2$). On the other hand, the EPR spectrum of ($TMTMP^{+\bullet}$)Fe^{IV}O(3-F-4-NO_2-PhO) was different from that of [($TMTMP^{+\bullet}$)Fe^{IV}O(2-MeIm)]$^+$ and exhibited an EPR signal at around $g \sim 2.0$ (Supporting Information, Figure S12), which was attributed to very weak magnetic interaction between iron(IV) and porphyrin radical spins. The EPR spectrum of ($TMTMP^{+\bullet}$)Fe^{IV}O(3-F-4-NO_2-PhO) was close to that of compound I of *Pm*-CAT.[10] The magnetic interactions between ferryl iron and the porphyrin

(32) Fujii, H.; Yoshimura, T.; Kamada, H. *Inorg. Chem.* **1996**, *35*, 2373–2377.

Table 3. ^{1}H NMR Chemical Shifts (ppm) and EPR Data of $(TMP^{+\bullet})Fe^{IV}O(L)$

L	*T*, °C	pyrrole-H	*ortho*-CH_3	*meta*-H	*para*-CH_3	*g*	*E*/*D*
Im[a]	−60	−10.4	22.8, 23.8	63.9, 65.4	10.3	4.41, 3.55, 1.98	0.070
	−80	−11.3	26.4, 27.5	73.1, 74.8	11.7		
2-MeIm[a]	−60	−8.8	25.6	70.6, 72.2	10.8	4.47, 3.45, 1.97	0.085
	−80	−9.8	broad	broad	11.3		
5-MeIm[a]	−60	−9.8	22.8, 24.0	64.4, 65.8	10.4	4.42, 3.57, 1.98	0.070
	−80	−11.1	24.2, 25.8	73.2, 74.9	11.2		
3-F-4-NO_2-PhO	−80	−13.7	25.4, 26.9	71.7	11.3	4.59, 3.40, 1.95	0.100
ClO_4^-	−80	−27.4	26.4, 23.9	66.4	11.3	4.42, 3.55, 1.98	0.075
NO_3^-	−80	−19.4	25.3, 27.8	72.5	10.2	4.45, 3.45, 1.96	0.090

[a] Counter anion is perchlorate ion (ClO_4^-). NMR; in dichloromethane-d_2. EPR; in dichloromethane-toluene (5:1) at 4 K.

Table 4. ^{1}H NMR Chemical Shifts (ppm) and EPR Data of $(TMTMP^{+\bullet})Fe^{IV}O(L)$

L	pyrrole-CH_3	meso-H	*ortho*-CH_3	*meta*-H	*para*-CH_3	*g*	J/D
Im[a]	113.2	0.0	7.5, 8.7	12.6, 13.4	3.2	2.97, 2.00	0.3
2-MeIm[a]	123.7	−14.8	8.0, 9.3	14.2, 15.0	2.9	3.67, 2.00	0.7
5-MeIm[a]	111.8	−4.0	7.4, 8.6	12.6, 13.4	3.1	3.84, 2.00	0.9
3-F-4-NO_2-PhO	101.9	−1.0	6.6, 7.7	13.3, 13.7	3.2	2.0	0
ClO_4^-	135.5	55.6	7.6, 9.6	14.2, 15.0	3.6	3.23, 2.00	0.4
NO_3^-	127.7	34.7	7.4, 8.3	13.8, 14.6	3.3	3.69, 2.00	0.7
	132.1	45.8	8.3, 9.6	13.7, 14.6	3.4		

[a] Counter anion is perchlorate ion (ClO_4^-). NMR; in dichloromethane-d_2. EPR; in dichloromethane-toluene (5:1) at 4 K.

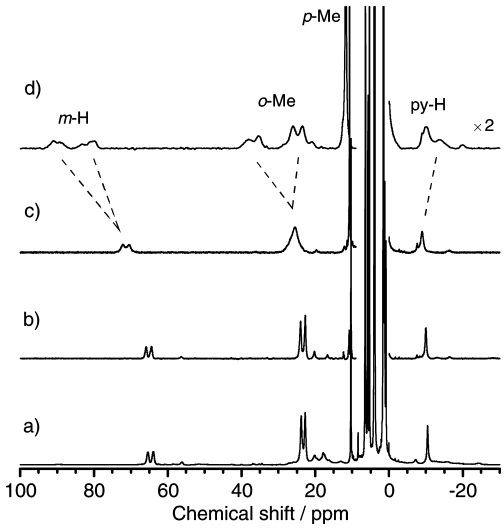

Figure 5. ^{1}H NMR spectra of $[(TMP^{+\bullet})Fe^{IV}O(L)](ClO_4)$ in dichloromethane-d_2 at −60 °C. (a) L = Im, (b) L = 5-MeIm, (c) L = 2-MeIm, (d) L = 2-MeIm at −90 °C.

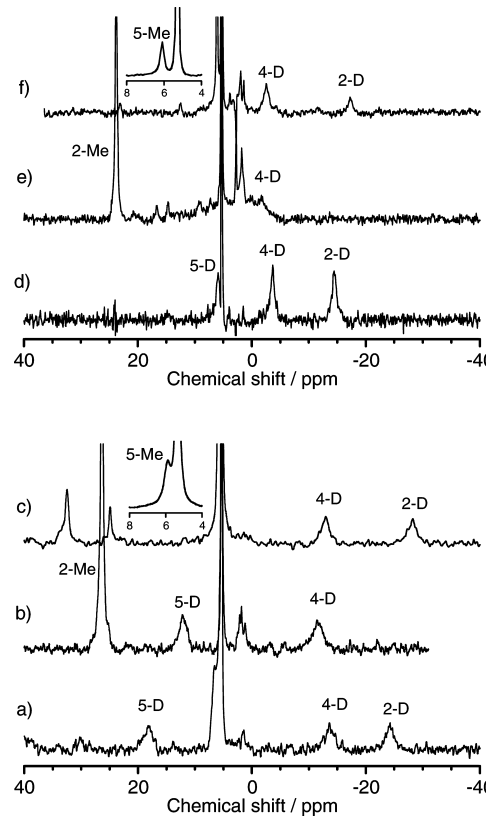

Figure 6. ^{2}H NMR spectra of (a) $[(TMP^{+\bullet})Fe^{IV}O(Im\text{-}d_4)](ClO_4)$, (b) $[(TMP^{+\bullet})Fe^{IV}O(2\text{-}MeIm\text{-}d_6)](ClO_4)$, (c) $[(TMP^{+\bullet})Fe^{IV}O(5\text{-}MeIm\text{-}d_6)](ClO_4)$, (d) $[(TMTMP^{+\bullet})Fe^{IV}O(Im\text{-}d_4)](ClO_4)$, (e) $[(TMTMP^{+\bullet})Fe^{IV}O(2\text{-}MeIm\text{-}d_6)](ClO_4)$, and (f) $[(TMTMP^{+\bullet})Fe^{IV}O(5\text{-}MeIm\text{-}d_6)](ClO_4)$ in dichloromethane. Temperature; (a−c) at −60 °C and (d−f) at −80 °C.

π-radical for TMTMP complexes were weaker than those for TMP complexes and became much weaker when the axial ligand was changed from imidazole to phenolate.

The structural characterization of oxoiron(IV) porphyrin π-cation radical complexes having imidazole and phenolate derivatives was examined using ESI-MS spectroscopy. ESI-MS peaks corresponding to $[(TMP^{+\bullet})Fe^{IV}O(L)]^+$ and $[(TMTMP^{+\bullet})Fe^{IV}O(L)]^+$ cations, where L = Im, 2-MeIm, and 5-MeIm, were detected (Supporting Information, Figure S13 and Table S1). The isotope distribution patterns of the observed ESI-MS peaks were almost identical to those calculated from $[(TMP^{+\bullet})Fe^{IV}O(L)]^+$ and $[(TMTMP^{+\bullet})Fe^{IV}O(L)]^+$ structures. All of the ESI-MS data supported the binding of imidazole derivatives as an axial ligand. On the other hand, ESI-MS ion peaks corresponding to $(TMP^{+\bullet})Fe^{IV}O(3\text{-}F\text{-}4\text{-}NO_2\text{-}PhO)$ and $(TMTMP^{+\bullet})Fe^{IV}O(3\text{-}F\text{-}4\text{-}NO_2\text{-}PhO)$ could not be detected because of their neutral character.

Reactivity of Compound I Models. To study the effect of axial ligands on reactivity, we examined reactions of oxoiron(IV) porphyrin π-cation radical complexes having various axial ligands with cyclooctene. Figure 8a and 8b shows the absorption spectral changes for the epoxidation reactions of $[(TMP^{+\bullet})Fe^{IV}O(Im)](NO_3)$ and $[(TMTMP^{+\bullet})Fe^{IV}O(Im)](NO_3)$ with cyclooctene at −80 °C, respectively. Upon the addition of cyclooctene, the absorption spectra of $[(TMP^{+\bullet})$-

Table 5. NMR Chemical Shifts (ppm) of Iron-Bound Imidazole Signals of Iron Porphyrin Complexes in Dichloromethane

complex	2-H(D)	4-H(D)	5-H(D)	*T*/°C	ref
$(TMP^{+\bullet})Fe^{IV}O(Im\text{-}d_4)^a$	−30.2	−17.4	19.1	−80	
$(TMP^{+\bullet})Fe^{IV}O(2\text{-}MeIm\text{-}d_6)^a$	29.4[d]	−15.0	12.4	−80	
$(TMP^{+\bullet})Fe^{IV}O(5\text{-}MeIm\text{-}d_6)^a$	−34.3	−17.4	6.1[d]	−80	
$(TMTMP^{+\bullet})Fe^{IV}O(Im\text{-}d_4)^a$	−14.5	−3.7	5.9	−80	
$(TMTMP^{+\bullet})Fe^{IV}O(2\text{-}MeIm\text{-}d_6)^a$	23.9[d]	−2.7	n.d.[e]	−80	
$(TMTMP^{+\bullet})Fe^{IV}O(5\text{-}MeIm\text{-}d_6)^a$	−17.3	−2.5	6.1[d]	−80	
$(TMP)Fe^{IV}O(1\text{-}MeIm)^b$	−28.5	−21.6	−3.6	−80	
$(TMP)Fe^{IV}O(1,2\text{-}DiMeIm)^b$	n.d.[e]	−20.7	−4.1	−80	
$(TMTMP)Fe^{IV}O(1\text{-}MeIm)^b$	−29.1	−22.7	−4.2	−80	
$(TMTMP)Fe^{IV}O(1,2\text{-}DiMeIm)^b$	n.d.[e]	n.d.[e]	−3.8	−80	
$(TmTP)Fe^{IV}O(1\text{-}MeIm\text{-}d_6)^c$	−22.5	−17.5	−2.8	−50	38
$(TmTP)Fe^{IV}O(1,2\text{-}DiMeIm\text{-}d_8)^c$	n.d.[e]	−13.7	−1.7	−50	38
$(TmTP)Fe^{IV}O(1,5\text{-}DiMeIm\text{-}d_8)^c$	−23.5	−15.8	−1.3[d]	−50	38
$(TMP)Fe^{III}(Im\text{-}d_4)^{a,f}$	−28.6	33.6	111.7	−60	
$(TMP)Fe^{III}(2\text{-}MeIm\text{-}d_6)^{a,f}$	18.4[d]	42.3	89	−60	
$(TMP)Fe^{III}(5\text{-}MeIm\text{-}d_6)^{a,f}$	−36.3	33.8	24.6[d]	−60	
$(TMTMP)Fe^{III}(Im\text{-}d_4)^{a,f}$	−45.2	30.1	115.3	−80	
$(TMTMP)Fe^{III}(2\text{-}MeIm\text{-}d_6)^{a,f}$	20.3[d]	45.9	91.3	−80	
$(TMTMP)Fe^{III}(5\text{-}MeIm\text{-}d_6)^{a,f}$	−49.4	31.2	22.9[d]	−80	

[a] Counter anion is perchlorate ion (ClO_4^-). [b] NMR shifts of heme protons are summarized in Supporting Information, Table S2. [c] TmTP; Tetra-*m*-tolylporphyrin, in toluene-d_8. [d] Methyl signal. [e] Not determined. [f] Assignments of the signals are based on the methyl substitutions (see Supporting Information, Figure S6).

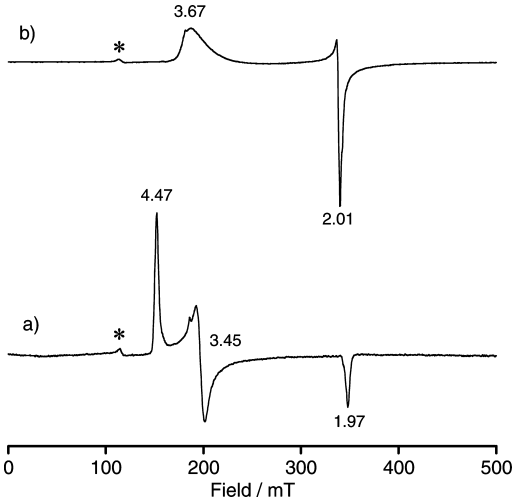

Figure 7. EPR spectra of (a) $[(P^{+\bullet})Fe^{IV}O(2\text{-}MeIm)](ClO_4)$ at 4K. (a) P = TMP, in dichloromethane-toluene (5:1), (b) P = TMTMP, in dichloromethane-propionitrile (5:1). Signals denoted by asterisks are due to $[(TMP)Fe^{III}(2\text{-}MeIm)](ClO_4)$ and $[(TMTMP)Fe^{III}(2\text{-}MeIm)](ClO_4)$.

$Fe^{IV}O(Im)](NO_3)$ and $[(TMTMP^{+\bullet})Fe^{IV}O(Im)](NO_3)$ changed to those of $(TMP)Fe^{III}(NO_3)$ and $(TMTMP)Fe^{III}(NO_3)$ containing 1 equiv of imidazole, respectively (Supporting Information, Figure S1). ^1H NMR measurements of the final reaction solutions clearly showed that the final product was a 1:1 mixture of nitrate and bis-imidazole iron(III) porphyrin complexes (Supporting Information, Figure S14). The absorption spectral changes for the reactions showed a slight shift in isosbestic points because the reaction product changed from the monoimidazole complex to a mixture of nitrate and bis-imidazole complexes, as the reaction product increased (Scheme 2). Similar absorption spectral changes were observed for cyclooctene epoxidation reactions when 2-methylimidazole and 4(5)-methylimidazole were used as axial ligands. In spite of a slight shift in the isosbestic points, the time courses of the absorptions for the epoxidation reactions in the presence of large excess of cyclooctene could be fitted well with a single exponential function.[33] The apparent rate constants linearly depend on the concentration of cyclooctene (Supporting Information, Figure S15), giving the second-order rate constants for cyclooctene epoxidation reactions (Table 6). To confirm the formation of the epoxidation product, GC-MS analysis was applied to each reaction solution used in these kinetic experiments, which showed the formation of cyclooctene oxide in more than 80% yield (see Table 6).

We further examined the reactions of oxoiron(IV) porphyrin π-cation radical complexes with 3-fluoro-4-nitrophenolate as an axial ligand. Panels c and d of Figure 8 show absorption spectral changes for the reactions of $(TMP^{+\bullet})Fe^{IV}O(3\text{-}F\text{-}4\text{-}NO_2\text{-}PhO)$ and $(TMTMP^{+\bullet})Fe^{IV}O(3\text{-}F\text{-}4\text{-}NO_2\text{-}PhO)$, respectively, with cyclooctene at 193 K. Upon the addition of cyclooctene, the absorption spectra of $(TMP^{+\bullet})Fe^{IV}O(3\text{-}F\text{-}4\text{-}NO_2\text{-}PhO)$ and $(TMTMP^{+\bullet})Fe^{IV}O(3\text{-}F\text{-}4\text{-}NO_2\text{-}PhO)$ changed to those of $(TMP)Fe^{III}(3\text{-}F\text{-}4\text{-}NO_2\text{-}PhO)$ and $(TMTMP)Fe^{III}(3\text{-}F\text{-}4\text{-}NO_2\text{-}PhO)$ with clear isosbestic points. The formation of $(TMP)Fe^{III}(3\text{-}F\text{-}4\text{-}NO_2\text{-}PhO)$ and $(TMTMP)Fe^{III}(3\text{-}F\text{-}4\text{-}NO_2\text{-}PhO)$ was further confirmed by ^1H NMR measurements. Kinetic analysis showed the second-order rate constants at 0.126 M^{-1} s^{-1} and 0.134 M^{-1} s^{-1} for the cyclooctene epoxidation with $(TMP^{+\bullet})Fe^{IV}O(3\text{-}F\text{-}4\text{-}NO_2\text{-}PhO)$ and $(TMTMP^{+\bullet})Fe^{IV}O(3\text{-}F\text{-}4\text{-}NO_2\text{-}PhO)$, respectively (Supporting Information, Figure S15). Analysis of the product using GC-MS showed that only cyclooctene oxide was detected, in 32 and 80% yield for $(TMP^{+\bullet})Fe^{IV}O(3\text{-}F\text{-}4\text{-}NO_2\text{-}PhO)$ and $(TMTMP^{+\bullet})Fe^{IV}O(3\text{-}F\text{-}4\text{-}NO_2\text{-}PhO)$, respectively. The low yield of cyclooctene oxide for $(TMP^{+\bullet})Fe^{IV}O(3\text{-}F\text{-}4\text{-}NO_2\text{-}PhO)$ may be due to its instability, as described in the section above.

The reaction rates of oxoiron(IV) porphyrin π-cation radical complexes with nitrate and chloride axial anions were also determined at 193 K (Supporting Information, Figures S15 and S16). The second-order rate constants and the yields of cyclooctene oxide are summarized in Table 6. The reaction of $(TMTMP^{+\bullet})Fe^{IV}O(Cl)$ could not be examined because the ozone oxidation of $(TMTMP)Fe^{III}Cl$ at −80 °C did not form $(TMTMP^{+\bullet})Fe^{IV}O(Cl)$. The reaction rate constants and reaction yields for imidazole and phenolate complexes were much larger than those for nitrate and chloride. In the most extreme case, the reaction rate was ∼400 times larger with the coordination of 2-methylimidazole to $(TMTMP^{+\bullet})Fe^{IV}O(NO_3)$.

To study the axial ligand effect on oxidation reactions other than epoxidation, we examined the reactions of oxoiron(IV) porphyrin π-cation radical complexes with *N*,*N*-dimethyl-*p*-nitroaniline and 1,4-cyclohexadiene (Table 6 and Supporting Information, Figure S17). Previous studies reported that oxoiron(IV) porphyrin π-cation radical complexes oxidize *N*,*N*-dimethyl-*p*-nitroaniline to *N*-methyl-*p*-nitroaniline via an electron transfer mechanism and 1,4-cyclohexadiene to benzene via

(33) Time course of the absorptions for $[(TMP^{+\bullet})Fe^{IV}O(5\text{-}MeIm)](NO_3)$ could not be fit well with a single exponential function, but with a bi-exponential function, suggesting some sequential reaction. The rate constant for the first reaction was assigned as that for $[(TMP^{+\bullet})Fe^{IV}O(5\text{-}MeIm)](NO_3)$ with cyclooctene.

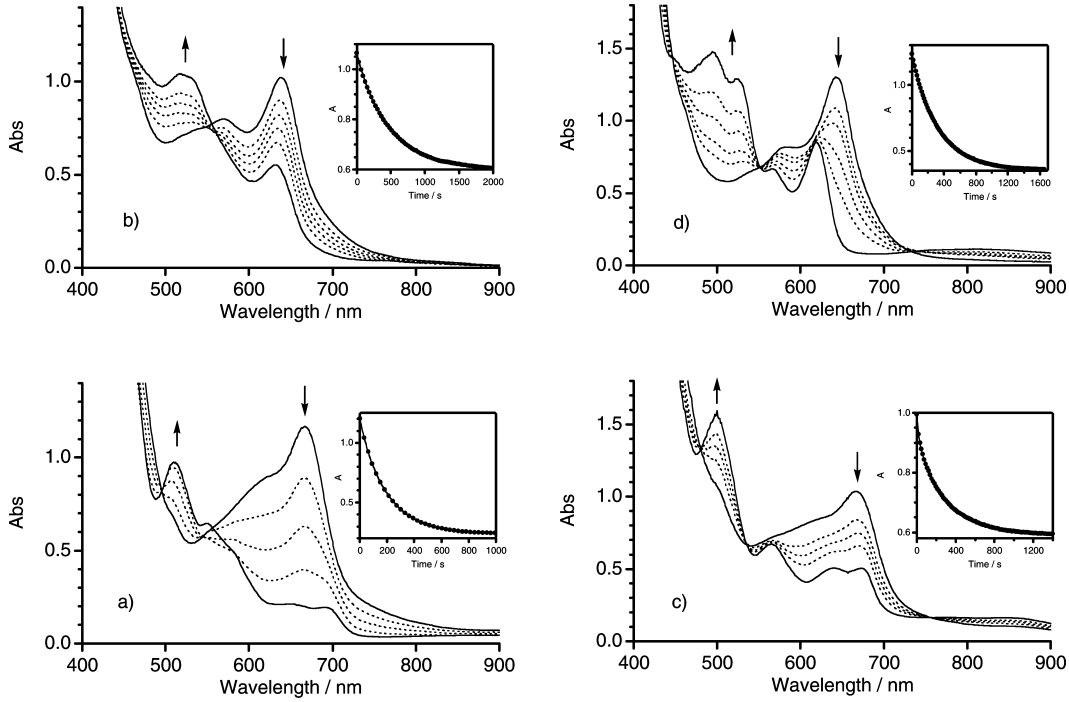

Figure 8. UV−visible absorption spectral change for the reactions of (a) [(TMP$^{+\bullet}$)Fe^{IV}O(Im)](NO$_3$), (b) [(TMTMP$^{+\bullet}$)Fe^{IV}O(Im)](NO$_3$), (c) (TMP$^{+\bullet}$)Fe^{IV}O(3-F-4-NO$_2$-PhO), and (d) (TMTMP$^{+\bullet}$)Fe^{IV}O(3-F-4-NO$_2$-PhO) with cyclooctene (2.5×10^{-2} M) in dichloromethane at −80 °C. Sample concentration = 1.0×10^{-4} M in 1 cm path length cell. Insets; time dependence of the absorptions at (a) 667 nm, (b) 639 nm, (c) 667 nm, and (d) 643 nm.

Scheme 2

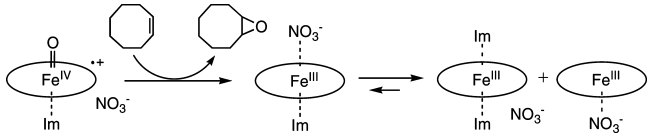

a hydrogen abstraction mechanism.[34,35] The second-order rate constants of [(TMTMP$^{+\bullet}$)Fe^{IV}O(Im)](NO$_3$) and (TMTMP$^{+\bullet}$)-Fe^{IV}O(3-F-4-NO$_2$-PhO) for *N*,*N*-dimethyl-*p*-nitroaniline were 70 times higher than that of (TMTMP$^{+\bullet}$)Fe^{IV}O(NO$_3$), and those for 1,4-dihydrocyclohexadiene were 10 times higher. Coordination of imidazole and phenolate axial ligands enhanced the reactivity of oxoiron(IV) porphyrin π-cation radical complex not only for the epoxidation reaction but also for the aniline *N*-demethylation and hydrogen abstraction reactions.

Regarding the catalase reactions, we examined the reactions of (TMTMP$^{+\bullet}$)Fe^{IV}O(NO$_3$), [(TMTMP$^{+\bullet}$)Fe^{IV}O(Im)](NO$_3$), and (TMTMP$^{+\bullet}$)Fe^{IV}O(3-F-4-NO$_2$-PhO) with hydrogen peroxide in dichloromethane at −80 °C. Whereas (TMTMP$^{+\bullet}$)Fe^{IV}O(NO$_3$) reacted in a few minutes with the addition of 10 equiv of hydrogen peroxide in methanol ($k_{app} = 2.0 \times 10^{-2}$ s^{-1} for 1 mM hydrogen peroxide), [(TMTMP$^{+\bullet}$)Fe^{IV}O(Im)](NO$_3$), and (TMTMP$^{+\bullet}$)Fe^{IV}O(3-F-4-NO$_2$-PhO) reacted immediately to form iron(III) porphyrin complexes. Because these reactions occurred so rapidly, the reaction rate constants could not be determined. While a drastic axial ligand effect was found for the hydrogen peroxide oxidation, predominance of the phenolate axial ligand over the imidazole axial ligand was not observed.

Discussion

Effect of Axial Ligand on Electronic Structure. All oxoiron(IV) porphyrin π-cation radical complexes characterized in this study showed the Soret band with decreased intensity around 400 nm and a characteristic absorption around 650 nm. The peak positions for TMP complexes were hardly changed by the axial ligand effect, however, those for TMTMP complexes were sensitive to the axial ligand effect (Table 1). In particular, the absorption peak at around 650 nm for TMTMP complexes showed ∼35 nm shift due to the axial ligand. It is worth noting that the peak position of (TMTMP$^{+\bullet}$)Fe^{IV}O(L) shifted to lower energy as the pK_a value of the axial ligand (L) increased (Figure 9).[36] The axial anion ligands showed a good correlation, while the axial neutral ligands, L = Im, 2-MeIm, and 5-MeIm, exhibited slight shifts from the correlation for the axial anion ligands. The absorption peak at around 650 nm may be a good marker for estimation of the electron donor ability of the axial ligand. Because of the structural similarity of protoporphyrin IX with TMTMP, a similar correlation was also observed for peak positions of compound I of peroxidases and catalases (Table 1 and 2). The peak positions of the compound I of peroxidases and catalases also shifted from 650 to 688 nm and were correlated with the pK_a values of the proximal ligands (Figure 9). Although other factors, such as the steric and electrostatic environment around heme, must be con-

(34) (a) Goto, Y.; Watamabe, Y.; Fukuzumi, S.; Jones, J. P.; Dinnocenzo, J. P. *J. Am. Chem. Soc.* **1998**, *120*, 10762–10763. (b) Chiavarino, B.; Cipollini, R.; Crestonei, M. E.; Fornarini, S.; Lanucara, F.; Lapi, A. *J. Am. Chem. Soc.* **2008**, *130*, 3208–3217.

(35) Jeong, Y. J.; Kang, Y.; Han, A.-R.; Lee, Y.-M.; Kotani, H.; Fukuzumi, S.; Nam, W. *Angew. Chem., Int. Ed.* **2008**, *47*, 7321–7324.

(36) (a) Albert, A. In *Physical Methods in Heterocyclic Chemistry*; Katritzky, A. R., Ed.; Academic Press: New York, 1971; Vol. III, pp 1−108. (b) Pine, S. H.; Hendrickson, J. B.; Vram, D. J.; Hammond, G. S. In *Organic Chemistry*, 4th ed; MacGraw-Hill: Auckland, 1981; Chapter 6, pp 196−239. (c) Albert, A.; Serjeant, E. P. In *The Determination of Ionization Constants*, 3rd ed.; Chapman and Hall: London, 1962; Chapter 9, pp 136−175. (d) Chapman, E.; Bryan, M. C.; Wong, C.-H. *Proc. Natl. Acad. Sci. U.S.A.* **2003**, *100*, 910–915.

Table 6. Second-Order Rate Constants for the Reaction of $(P^{+\cdot})Fe^{IV}O(L)$ with the Various Substrates in CH_2Cl_2 at −80 °C

		k_2, M^{-1} s^{-1}		
porphyrin	ligand	cyclooctene[a]	1,4-cyclohexadiene	*N*,*N*-dimethyl-*p*-nitroaniline
TMP	Im	0.216 ± 0.003 (87 ± 3)		
	2-MeIm	0.030 ± 0.002 (72 ± 4)		
	5-MeIm	0.240 ± 0.003 (71 ± 3)		
	3-F-4-NO_2-PhO[b]	0.126 ± 0.001 (32 ± 8)		
	Cl^-	0.011 ± 0.001 (62 ± 2)		
	NO_3^-	$8.21 \pm 0.31 \times 10^{-4}$ (64 ± 2)		
TMTMP	Im	0.095 ± 0.001 (82 ± 2)	0.868 ± 0.005	3.470 ± 0.225
	2-MeIm	0.306 ± 0.002 (89 ± 3)		
	5-MeIm	0.126 ± 0.001 (67 ± 5)		
	3-F-4-NO_2-PhO	0.134 ± 0.001 (80 ± 3)	1.043 ± 0.016	3.383 ± 0.050
	NO_3^-	$7.13 \pm 0.25 \times 10^{-4}$ (48 ± 1)	0.082 ± 0.005	0.048 ± 0.002

[a] Numbers in parentheses are yield (%) of cyclooctene oxide. [b] Rate for the second slow reaction was 0.020 ± 0.001 M^{-1} s^{-1}.[31]

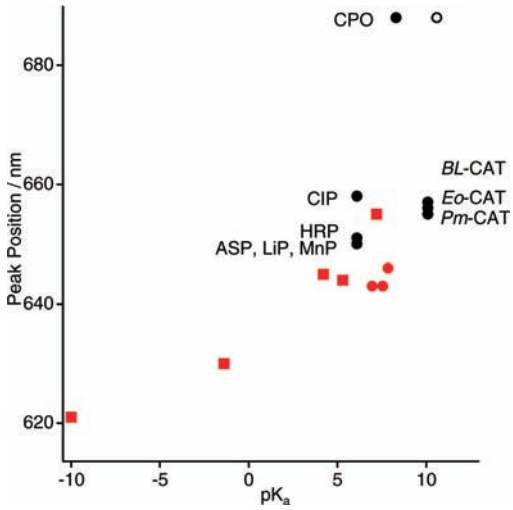

Figure 9. Correlation of pK_a value of the axial ligand (L) of $(TMTMP^{+\cdot})Fe^{IV}O(L)$ with its absorption peak position. Red square; anion ligand, L from left; ClO_4^-, NO_3^-, benzoate, 3-F-4-NO_2-PhO, 4-NO_2-PhO, red circle; neutral ligand, L from left; Im, 5-MeIm, 2-MeIm. Black circle; compound-I of heme enzymes listed in Table 1. The pK_a values for peroxidases other than CPO, catalases, and CPO are used those for histidine (6.1), tyrosine (10.1), and cysteine (8.3) residues, respectively.[36] Circle; CPO compound-I for the pK_a (10.6) of ethanethiol.[36]

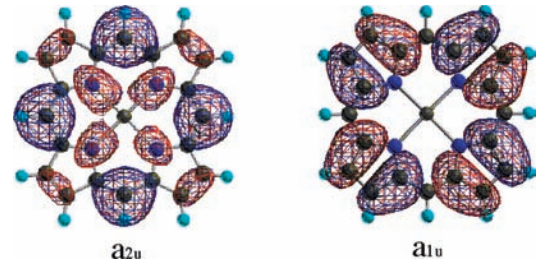

Figure 10. Electron spin density distribution of the a_{2u} and a_{1u} porphyrin π-cation radical orbitals. Red and blue colors represent signs of wave functions.

sidered, the peak position observed for compound I can be explained by the donor effect of the proximal ligand in these heme enzymes. For peroxidases other than CPO, the observed peak positions (650−658 nm) were close to the correlation for the axial anion ligands and were reasonable for the character of the imidazolate anion, resulting from hydrogen bonding interactions of the proximal histidines with the aspartate residues (see Figure 1a). The peak positions (655−657 nm) for catalases can be explained by hydrogen bonding between the proximal tyrosine ligand (phenolate) and a nearby arginine residue (see Figure 1b), which shifted the phenolate character of the proximal ligand to a phenol and weakens the electron donor effect of the proximal tyrosine ligand. The absorption peak (688 nm) for CPO compound I indicates extremely strong electron donor effect of the proximal cysteine ligand. The donor effect was much stronger than that expected from the pK_a value (8.3) of cysteine but comparable to that expected from alkylthiol (pK_a 10−11).[36]

Previously, we showed that the porphyrin π-cation radical (a_{1u} or a_{2u}) state depends on the porphyrin substitution pattern (Figure 10).[31a] Meso-substituted porphyrins, such as TMP, form the a_{2u} radical state, which shifts to the a_{1u} state with an increase in the electron-withdrawing effect of the meso-substituent. Pyrrole β-substituted porphyrins, like TMTMP, form the a_{1u} radical state, which is not changed even with an increase in the electron-withdrawing effect of the pyrrole β-substituent. On the other hand, the present ^{1}H NMR results clearly show that the axial ligand effect does not change the porphyrin π-cation radical state. Even if the electron-donating axial ligand, such as imidazole and phenolate, were coordinated to the ferryl iron, TMTMP and TMP complexes remained in the a_{1u} and a_{2u} radical states, respectively. These results indicate that compound I in all peroxidases and catalases with pyrrole β-substituted porphyrin, like protoporphyrin IX, would be in the a_{1u} radical state because one-electron oxidation of protoporphyrin IX usually yields the a_{1u} radical state.

The paramagnetic shifts of the iron-bound axial ligands allow the estimation of spin transfer from ferryl iron and porphyrin π-cation radical spins to the iron-bound oxo and axial ligand. The radical character of the oxo ligand has been discussed in relation to the oxygenation reactivity of oxoiron(IV) porphyrin π-cation radical complex,[37] but the spin transfer from the porphyrin π-cation radical to the axial ligand has not been studied in detail. As summarized in Figure 6 and Table 5, the iron-bound imidazole signals showed paramagnetic shifts, induced by ferryl iron and porphyrin π-cation radical spins. We assume here that the dipolar contribution of oxoiron(IV) porphyrin π-cation

(37) (a) Groves, J. T.; Nemo, T. E. *J. Am. Chem. Soc.* **1983**, *105*, 6243–6248. (b) Champion, P. M. *J. Am. Chem. Soc.* **1989**, *111*, 3434–3436. (c) Bernadou, J.; Fabiano, A.-S.; Robert, A.; Meunier, B. *J. Am. Chem. Soc.* **1994**, *116*, 9375–9376.
(38) Balch, A. L.; La Mar, G. N.; Latos-Grazynski, L.; Renner, M. W.; Thanabal, V. *J. Am. Chem. Soc.* **1985**, *107*, 3003–3007.

radical complex is close to that of oxoiron(IV) porphyrin complex.[38] As previously analyzed for oxoiron(IV) porphyrin complexes, two unpaired electrons in the ferryl iron d_π (d_{xz} and d_{yz}) orbitals delocalize into the imidazole π-orbital (the highest occupied π-molecular orbital), leading to upfield shifts of all protons belonging to the iron-bound imidazoles.[38] On the other hand, porphyrin π-cation radical spin would be transferred to the axial imidazole σ-orbital via the unoccupied ferryl iron d_{z^2} orbital, resulting in downfield shifts of the imidazole signals, especially the imidazole 1-H and 5-H signals, as observed for high spin iron(III) porphyrin complexes (see Table 5 and Supporting Information, Figure S9).[39] Therefore, the upfield shifts of the imidazole 2-H and 4-H signals for oxoiron(IV) porphyrin π-cation radical complexes were mainly induced by the spin delocalization of the ferryl iron d_π spins. This result was further confirmed by the large downfield shifts with the 2-methyl substitutions. Compared with the NMR shifts of the iron-bound imidazole signals of oxoiron(IV) porphyrin complexes, the upfield shifts of the imidazole 2-H and 4-H signals for TMTMP complexes become smaller with the formation of porphyrin π-cation radicals, while those for TMP complexes hardly change. Since the NMR shifts of the iron-bound imidazole signals of oxoiron(IV) TMP complexes were similar to those of TMTMP complexes (Table 5), the observed change suggests that spin transfer of the ferryl iron spins to the axial ligands is weakened with the formation of the a_{1u} radical complex (TMTMP) but is unchanged with the formation of the a_{2u} radical complex (TMP). On the other hand, with the formation of the porphyrin π-cation radical, the imidazole 5-H(D) signals showed large downfield shifts for the TMP complexes, but small shifts for the TMTMP complexes. Large downfield shifts of the 5-H(D) signals for TMP complexes indicate effective spin transfer from the a_{2u} porphyrin radical, but the small shifts for TMTMP complexes indicate ineffective transfer from the a_{1u} porphyrin radical. Overall, the ferryl iron and porphyrin π-cation radical spins were effectively transferred to the axial imidazole for the a_{2u} radical complex, but not for the a_{1u} radical complex. This is consistent with a previous EPR study of zinc(II) porphyrin π-cation radical complexes.[40] With molecular vibration of the propyhrin plane, for example, doming, the a_{2u} orbital is allowed to overlap with the ferryl iron d_{z^2} orbital but the a_{1u} orbital is not. Moreover, the π-spin density of the pyrrole nitrogen is large in the a_{2u} orbital but not in the a_{1u} orbital (see Figure 10). These differences should result in differing spin transfer between the a_{1u} and a_{2u} complexes. This argument is applicable to the axial oxo ligand of oxoiron(IV) porphyrin π-cation radical complex, suggesting different spin density on the oxo ligand in the a_{1u} and a_{2u} radical complexes.

The effect of the axial ligand on spin interaction between the ferryl iron and porphyrin π-cation radical spins of oxoiron(IV) porphyrin π-cation radical complex is manifested in its EPR spectrum. The difference in spin interaction

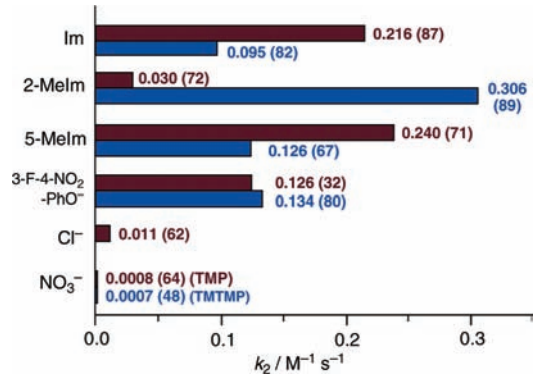

Figure 11. Comparison of second-order rate constants for the cyclooctene epoxidation of oxoiron(IV) TMP (brown bar) and TMTMP (blue bar) π-cation radical complexes with various axial ligands. The numbers in parentheses are yields of cyclooctene oxide.

between the TMP and TMTMP complexes might result from differences in both the π-spin density on the pyrrole nitrogen atom between the a_{2u} and a_{1u} radical states (see Figure 10) and the flexibility of the porphyrin plane of TMTMP because of less steric hindrance than in TMP. The EPR spectra of compound I in heme enzymes more closely resemble those of TMTMP complexes, confirming the a_{1u} radical state. The similarity of the EPR spectra of the compound I of heme enzymes with those of model complexes with similar axial ligands suggests that the axial ligand effect is an important determinant of the intramolecular spin interaction of the compound I, as well as the steric effect of amino acid residues around the heme.

Effect of the Axial Ligand on Reactivity. Previously, the axial ligand effect on styrene oxidation was studied using $(TMP^{+\bullet})Fe^{IV}O(X)$, where X is either chloride, fluoride, acetate, methanol, or trifluoromethylsulfonate.[18] The second-order rate constant for the styrene oxidation was increased about 15 times when the axial ligand was changed from the least reactive trifluoromethylsulfonate to the most reactive fluoride. In this study, we also found similar increments when the axial ligand was changed from nitrate to chloride (~15-fold). More importantly, this study showed a significant effect of axial ligands of imidazole and phenolate derivatives on the reactivity of oxoiron(IV) porphyrin π-cation radical complex. As clearly shown in Figure 11, the effect of the axial imidazole and phenolate was much more prominent than that of the axial chloride. For the 3-fluoro-4-nitrophenolate axial ligand, the second-order rate constants for the TMP and TMTMP complexes were comparable. However, for the imidazole and 4(5)-methylimidazole axial ligands, the second-order rate constants for the TMP complexes were about twice those of the TMTMP complexes. For the 2-methylimidazole axial ligand, the TMTMP complex was much more reactive than the TMP complex. The low reactivity of $(TMP^{+\bullet})Fe^{IV}O$(2-MeIm) may be due to steric interaction between the methyl groups of TMP and 2-methylimidazole, which was detected in its ^1H NMR spectra. As reported for 1,2-dimethylimidazole complexes of ferric TMP,[41] the steric interaction might induce ruffling of the

(39) Cheng, R.-J.; Chen, P.-Y.; Lovell, T.; Liu, T.; Noodleman, L.; Case, D. A. *J. Am. Chem. Soc.* **2003**, *125*, 6774–6783.

(40) Fujita, I.; Hanson, L. K.; Walker, F. A.; Fajer, J. *J. Am. Chem. Soc.* **1983**, *105*, 3296–3300.

(41) Munro, O. Q.; Marques, H. M.; Debrunner, P. G.; Mohanrao, K.; Scheidt, W. R. *J. Am. Chem. Soc.* **1995**, *117*, 935–954.

porphyrin plane of $(TMP^{+\bullet})Fe^{IV}O(2\text{-MeIm})$, leading to a drastic decrease in epoxidation reactivity.

A drastic axial ligand effect of imidazole and phenolate derivatives was also found in the reactions with 1,4-cyclohexadiene, *N*,*N*-dimethyl-*p*-nitroaniline, and hydrogen peroxide. However, the axial ligand effect (~10-fold) for 1,4-cyclohexadiene is not so significant as those (~100-fold) for *N*,*N*-dimethyl-*p*-nitroaniline and cyclooctene (Table 6). Although we attempted to correlate these reactivities with the present spectroscopic results of oxiron(IV) porphyrin π-cation radical complexes, we could not find any clear correlation. Therefore, the explanation for the dramatic axial ligand effect on the reactivity must be effects other than the electronic state of the oxiron(IV) porphyrin π-cation radical complex. For example, differences in the reaction mechanism, such as hydrogen abstraction and electron transfer, would form different transition states, which might result in different axial ligand effects. The axial ligand effect on oxoiron(IV) porphyrin π-cation radical complex would be different from that on iron(III) porphyrin complex as a reaction product. Moreover, the thermodynamic parameters for substrate oxidation must also be considered. For example, the change in an enthalpy (ΔH) for conversion of 1,4-cyclohexadine to benzene and water is ~ -260 kJ/mol, while that of cyclohexene to cyclohexene oxide is ~ -120 kJ/mol.[42] The large enthalpy contribution from the substrate oxidation would weaken the enthalpy contribution from the axial ligand effect.

Previously, the axial ligand effect of imidazole and phenolate has been reported in catalytic oxygenation reactions with iron and manganese porphyrin complexes.[12−17] Previously, Watanabe et al. studied the axial ligand effect on the former process, in which the coordination of the axial imidazole ligand increased the rate of the O−O bond cleavage of iron bound *m*-chloroperbenzoate and the rate correlated with the donor effect of the axial imidazole ligand.[5] On the other hand, this study clearly showed that the axial imidazole and phenolate ligands drastically increased the reaction rates of oxoiron(IV) porphyrin π-cation radical complexes with substrates. In the catalytic system, the axial ligand works to accelerate not only the formation of the high-valent oxo complex but also the oxo-transfer to substrate. This would be the same in the heme enzymes. The proximal histidine and tyrosine residues would drastically increase the reactivity of compound I, resulting in much more reactive compound I in peroxidases and catalases than in the synthetic model complexes. The very reactive compound I would lead to extremely high catalytic activity of these heme enzymes. Although this study does not show the effect of the thiolate axial ligand, the cysteine proximal ligands in cytochrome P450 may also work to enhance the oxo-transfer reactivity. Finally, in the oxidation reactions of cyclooctene, 1,4-cyclohexadiene, *N*,*N*-dimethyl-*p*-nitroaniline, and hydrogen peroxide, we could not find a significant difference between the imidazole and phenolate axial ligands. While the axial ligand activates the compound I in heme enzyme, the axial ligand would not be an essential factor to discriminate the enzyme function.

Experimental Section

Instrumentation. UV−visible absorption spectra were recorded on an Agilent 8453 (Agilent Technologies) equipped with a USP-203 low-temperature chamber (UNISOKU). ^{1}H, ^{2}H, ^{13}C, and ^{19}F NMR were measured on a Lambda-500 spectrometer (JEOL). ^{1}H, ^{2}H, and ^{13}C NMR chemical shifts were reported versus tetramethylsilane (TMS) and referenced to residual solvent peaks (dichloromethane: 5.32 ppm). ^{19}F chemical shift values were referenced to external hexafluorobenzene (C_6F_6) at 0 ppm. The concentrations of NMR samples were ~5 mM. EPR spectra were recorded at 4 K on Bruker E500 X-band spectrometer with an Oxford Instruments EPR910 helium-flow cryostat (Bruker). The concentrations of EPR samples were 1−3 mM. ESI-MS spectra were obtained with a LCT time-of-flight mass spectrometer equipped with an elecrospray ionization interface (Micromass). For oxoiron(IV) porphyrin π-cation radical complexes, desolvation and nebulizer gases were cooled with liquid nitrogen. The ESI-MS samples were prepared by oxidation with ozone in acetonitrile or dichloromethane at 233 K, followed by dilution with the same solvent, and injected into the ESI-MS with a gastight syringe cooled with dry ice. The sample solution was then transferred to the inlet of the mass spectrometer through a precooled capillary tube. Gas chromatography−mass spectroscopy (GC-MS) analysis was performed on a QP-5000 GC-MS system (Shimadzu) equipped with a capillary gas chromatograph (GC-17A, CBP5-M25−025 capillary column). Ozone gas was generated by UV irradiation of oxygen gas (99.9%) with an ozone generator PR-1300 (Clear Water) and used without further purification.

Materials. Imidazole-d_4 (98 atom % D) was purchased from Aldrich. 2-Methylimidazole-d_6 (98.1 atom % D) was purchased from CDN ISOTOPES (Canada). 4-Methylimidazole-d_6 was prepared from 4-methylimidazole by activated 10% Pd/C in D_2O, according to the literature.[43] Deuterium incorporation into 4-methylimidazole, as analyzed by ^{1}H and ^{13}C NMR, was 2-H (95%), 5-H (95%), and 4-methyl group (50%). Dichloromethane was purchased from a commercial company as the anhydrous solvent and was stored in the presence of 4A molecular sieves. Other chemicals were purchased from commercial companies and used without further purification. *meso*-Tetramesitylporphyrin ($TMPH_2$) and 2,7,12,17-teramethyl-3,8,13,18-tetramesitylporphyrin ($TMTMPH_2$) were prepared according to the literature.[44] $(TMP)Fe^{III}Cl$ and $(TMTMP)Fe^{III}Cl$ were prepared by the insertion of iron into $TMPH_2$ and $TMTMPH_2$ with $FeCl_2$ and sodium acetate in acetic acid, respectively, and purified by silica gel column using CH_2Cl_2/CH_3OH as an eluent. $(TMP)Fe^{III}OH$ and $(TMTMP)Fe^{III}OH$ were obtained from $(TMP)Fe^{III}Cl$ and $(TMTMP)Fe^{III}Cl$, respectively, by passing through a basic alumina (10% water) column with dichloromethane as an eluent.[45] $(TMP)Fe^{III}ClO_4$ and $(TMTMP)Fe^{III}ClO_4$ were prepared by the reaction of $(TMP)Fe^{III}Cl$ and $(TMTMP)Fe^{III}Cl$, respectively, with silver(I) perchlorate in dichloromethane solution, and purified by recrystallization from dichlo-

(42) (a) Pedley, J. B.; Naylor, R. D.; Kirby, S. P. *Thermochemical Data of Organic Compounds*; Chapman and Hall: London, 1986. (b) Stull, D. R.; Westrum, E. F.; Sinke, G. C. *The Chemical Thermodynamics of Organic Compounds*; John Wiley: New York, 1969. (c) Nagano, H. In *Kagaku-Binran*, 5th ed.; Atake, T., Sorai, M., Matsuo, T., Eds.; Maruzen: Tokyo; Vol. II, pp 301−313.

(43) Hardacre, C.; Holbrey, J. D.; McMath, S. E. J. *Chem. Commun.* **2001**, 367–368.

(44) (a) Lindsey, J.; Wagner, R. *J. Org. Chem.* **1989**, *54*, 828–836. (b) Ono, N.; Kawamura, H.; Bougauchi, M.; Maruyama, K. *Tetrahedron* **1990**, *46*, 7483–7496.

(45) Groves, J. T.; Gross, Z.; Stern, M. K. *Inorg. Chem.* **1994**, *33*, 5065–5072.

romethane/*n*-hexane.[46] (TMP)$Fe^{III}NO_3$ and (TMTMP)$Fe^{III}NO_3$ were obtained by mixing (TMP)Fe^{III}OH and (TMTMP)Fe^{III}OH in toluene with 1 M nitric acid, and purified by recrystallization from ether/*n*-hexane.[47] (TMP)$Fe^{III}(NO_3)$; ^{1}H NMR (CD_2Cl_2, 25 °C), 4.0 and 6.2 (*ortho*-Me), 15.3 and 16.5 (*meta*-H), 4.3 (*para*-Me), 74.0 (pyrrole-H). UV−vis. (CH_2Cl_2, 25 °C), 412, 514, 580, 647, and 691 nm. (TMTMP)$Fe^{III}(NO_3)$; ^{1}H NMR (CD_2Cl_2, 25 °C), −49.6 (meso-H), 5.1 and 8.4 (*ortho*-Me), 12.9 and 13.3 (*meta*-H), 6.3 (*para*-Me), 58.7 (pyrrole-Me). UV−vis. (CH_2Cl_2, 25 °C), 388, 506, 532, and 637 nm.

Synthesis. Iron(III) Phenolate Complexes. Iron(III) phenolate complexes were prepared by the published method.[48] (TMP)Fe^{III}OH and (TMTMP)Fe^{III}OH were dissolved in toluene and 1 equiv of phenol derivative (4-nitrophenol, pentafluorophenol, 3,4,5-trifluorophenol, or 3-fluoro-4-nitrophenol) was added with stirring. The green or red solution changed to brown as the phenol dissolved. The solution was evaporated to dryness, and the residue was purified by crystallization from ether/hexane. Microcrystals of the iron(III) phenol complex were collected by filtration. (TMP)Fe^{III}(4-NO_2-PhO); ^{1}H NMR (CD_2Cl_2, 25 °C), 3.0 and 5.2 (*ortho*-Me), 12.5 and 13.5 (*meta*-H), 3.7 (*para*-Me), 79.1 (pyrrole-H), −91.4 (phenol *ortho*-H), 83.0 (phenol *meta*-H). UV−vis. (CH_2Cl_2, 25 °C), 420, 497, 559, 635, and 667 nm. (TMP)Fe^{III}(F_5-PhO); ^{1}H NMR (CD_2Cl_2, 25 °C), 2.9 and 5.2 (*ortho*-Me), 12.7 and 13.6 (*meta*-H), 3.8 (*para*-Me), 78.7 (pyrrole-H). UV−vis. (CH_2Cl_2, 298 K), 415, 500, 566, 642, and 673 nm. (TMP)Fe^{III}(3,4,5-F_3-PhO); ^{1}H NMR (CD_2Cl_2, 25 °C), 3.0 and 5.1 (*ortho*-Me), 12.3 and 13.3 (*meta*-H), 3.7 (*para*-Me), 79.8 (pyrrole-H), −101.0 (phenol *ortho*-H). UV−vis. (CH_2Cl_2, 25 °C), 420, 490, 557, 620, and 666 nm. (TMP)Fe^{III}(3-F-4-NO_2-PhO); ^{1}H NMR (CD_2Cl_2, 25 °C), 3.1 and 5.2 (*ortho*-Me), 12.7 and 13.7 (*meta*-H), 3.8 (*para*-Me), 78.9 (pyrrole-H), −85.1 and −81.5 (phenol *ortho*-H), 72.4 (phenol *meta*-H). ^{19}F NMR (CD_2Cl_2, 25 °C), 58.4 (*meta*-F). UV−vis. (CH_2Cl_2, 25 °C), 419, 500, 560, 640, and 668 nm. (TMTMP)Fe^{III}(F_5-PhO); ^{1}H NMR (CD_2Cl_2, 25 °C), −40.5 (meso-H), 4.8 and 7.4 (*ortho*-Me), 11.9 and 12.0 (*meta*-H), 6.0 (*para*-Me), 47.7 (pyrrole-Me), −83.1 and −79.9 (phenol *ortho*-H), 67.9 (phenol *meta*-H). UV−vis. (CH_2Cl_2, 25 °C), 371, 398, 498, 526, and 619 nm. (TMTMP)Fe^{III}(3-F-4-NO_2-PhO); ^{1}H NMR (CD_2Cl_2, 25 °C), −47.0 (meso-H), 4.5 and 7.3 (*ortho*-Me), 11.9 and 12.0 (*meta*-H), 5.0 (*para*-Me), 47.0 (pyrrole-Me), −83.1 and −79.9 (phenol *ortho*-H), 67.9 (phenol *meta*-H). ^{19}F NMR (CD_2Cl_2, 25 °C), 58.3 (*meta*-F). UV−vis. (CH_2Cl_2, 25 °C), 370, 401, 496, 524, and 619 nm.

Iron(III) Monoimidazole Complexes. Iron(III) porphyrin monoimidazole complex was generated in situ by adding 1.0 equiv of imidazole, 2-methylimidazole, or 4-methylimidazole to perchlorate iron(III) porphyrin in dichloromethane.[49] [(TMP)Fe^{III}(Im)]ClO_4; ^{1}H NMR (CD_2Cl_2, 25 °C), 3.1 and 5.3 (*ortho*-Me), 12.6 and 13.4 (*meta*-H), 4.3 (*para*-Me), 19.9 (pyrrole-H), −15.5 (Im 2-H), 30.1 (Im 4-H), 85.1 (Im 5-H), 100.4 (Im N−H). UV−vis. (CH_2Cl_2, 25 °C), 412, 510, 575, and 690 nm. [(TMP)Fe^{III}(2-MeIm)]ClO_4; ^{1}H NMR (CD_2Cl_2, 298K), 2.7 and 5.7 (*ortho*-Me), 12.7 and 13.1 (*meta*-H), 4.1 (*para*-Me), 34.9 (pyrrole-H), 16.6 (2-MeIm 2-Me), 31.8 (2-MeIm 4-H), 65.8 (2-MeIm 5-H), 109.0 (2-MeIm N−H). UV−vis. (CH_2Cl_2, 25 °C), 412, 511, 572 and 692 nm. [(TMP)Fe^{III}(5-MeIm)]ClO_4; ^{1}H NMR (CD_2Cl_2, 25 °C), 13.0 and 13.9 (*meta*-H), 4.4 (*para*-Me), 31.7 (pyrrole-H), −18.6 (5-MeIm 2-Me), 31.7 (5-MeIm 4-H), 22.0 (5-MeIm 5-Me), 100.8 (5-MeIm N−H). UV−vis. (CH_2Cl_2, 25 °C), 412, 510, 572, and 692 nm. [(TMTMP)Fe^{III}-(Im)]ClO_4; ^{1}H NMR (CD_2Cl_2, 25 °C), −16.6 (meso-H), 4.8 and 8.0 (*ortho*-Me), 13.5 and 14.4 (*meta*-H), 5.5 (*para*-Me), 69.2 (pyrrole-Me), −16.1 (Im 2-H), 31.2 (Hm 4-H), 82.6 (Im 5-H), 98.5 (Im N−H). UV−vis. (CH_2Cl_2, 25 °C), 385, 503, and 626 nm. [(TMTMP)Fe^{III}(2-MeIm)]ClO_4; ^{1}H NMR (CD_2Cl_2, 25 °C), −31.9 (meso-H), 5.1 and 8.8 (*ortho*-Me), 13.8 and 14.5 (*meta*-H), 6.2 (*para*-Me), 70.0 (pyrrole-Me), 17.5 (2-MeIm 2-Me), 35.9 (2-MeIm 4-H), 66.6 (2-MeIm 5-H), 110.0 (2-MeIm N−H). UV−vis. (CH_2Cl_2, 298K), 385, 503, and 626 nm. [(TMTMP)Fe^{III}(5-MeIm)]ClO_4; ^{1}H NMR (CD_2Cl_2, 298 K), −20.1 (meso-H), 5.0 and 8.2 (*ortho*-Me), 13.7 and 14.5 (*meta*-H), 5.8 (*para*-Me), 70.3 (pyrrole-Me), −15.4 (5-MeIm 2-H), 32.6 (5-MeIm 4-H), 20.7 (5-MeIm 5-H), 99.5 (5-MeIm N−H). UV−vis. (CH_2Cl_2, 25 °C), 385, 503, and 626 nm.

Oxoiron(IV) Porphyrin Complexes. Oxoiron(IV) porphyrin complexes were prepared as previously described.[45] (TMP)-$Fe^{III}(ClO_4)_2$ or (TMTMP)$Fe^{III}(ClO_4)_2$, which was prepared from the oxidation of (TMP)Fe^{III}OH or (TMTMP)Fe^{III}OH with solid ferric perchlorate, in dichloromethane-d_2 was transferred through a short basic alumina (20% water) column (0.5 × 1 cm) at ambient temperature, directly into a NMR tube in dry ice-acetone bath. One equiv of 1-MeIm or 1,2-DiMeIm in dichloromethane-d_2 was slowly added to the cooled solution in the NMR tube.

Ozone Oxidation of Iron(III) Porphyrin. For NMR or EPR measurement, iron(III) porphyrin complexes were dissolved in dichloromethane and placed in NMR or EPR cell. The solution was cooled by a dry ice acetone bath. Ozone gas was slowly bubbled in the solution with a gastight syringe. With the formation of oxoiron(IV) porphyrin π-cation radical complexes, the brown solution changed to green. The oxidations were monitored by ^{1}H NMR or EPR spectra. For UV−visible absorption spectra, the oxidation was carried out in a 1 cm quartz cuvette in a low-temperature chamber set with a UV−visible absorption spectrometer and monitored by absorption spectral change. Finally, excess ozone gas was removed by bubbling argon gas with a gastight syringe.

Kinetics and Product Analysis. Oxoiron(IV) porphyrin π-cation radical (100 μM) in dichloromethane was prepared in a 1 cm quartz cuvette in a low-temperature chamber set with a UV−visible absorption spectrometer, as described above. An excess of cyclooctene (20−1000 equiv) was then added to the solution with vigorous stirring, and the reactions were monitored by the absorption spectral change at constant time intervals. After confirming the completion of the reactions, 10 equiv of tetrabutylammonium iodide (n-$Bu_4N^+I^-$) was added to the solution at the same temperature. After warming to room temperature, quantitative product analyses were subsequently performed with GC-MS using undecane as an internal standard. The reaction rate constants were determined by computer simulation of absorption versus time for the reactions.

Acknowledgment. This work was supported by grants from the Japan Science and Technology Agency, CREST, and from the Ministry of Education, Culture, Sports, Science and Technology, Japan, the Global COE program.

Supporting Information Available: Text (PDF) containing additional figures (Figure S1−S17) and tables (Tables S1 and S2). This material is available free of charge via the Internet at http://pubs.acs.org.

IC802123M

(46) Reed, C. A.; Mashiko, T.; Bentley, S. P.; Kastner, M. E.; Scheidt, W. R.; Spartalian, K.; Lang, G. *J. Am. Chem. Soc.* **1979**, *101*, 2948–2958.

(47) Phillippi, M. A.; Baenziger, N.; Goff, H. M. *Inorg. Chem.* **1981**, *20*, 3904–3911.

(48) (a) Tang, S. C.; Koch, S.; Papaefthymiou, G. C.; Foner, S.; Frankel, R. B.; Ibers, J. A.; Holm, R. H. *J. Am. Chem. Soc.* **1976**, *98*, 2414–2434. (b) Ainscough, E. W.; Addison, A. W.; Dolphin, D.; James, B. R. *J. Am. Chem. Soc.* **1978**, *100*, 7585–7591.

(49) (a) Quinn, R.; Nappa, M.; Valentine, J. S. *J. Am. Chem. Soc.* **1982**, *104*, 2588–2595. (b) Scheidt, W. R.; Geiger, D. K.; Lee, Y. J.; Reed, C. A.; Lang, G. *J. Am. Chem. Soc.* **1985**, *107*, 5693–5699.